vehicles

MDPI

Article

Adaptive Robust Terminal Sliding Mode Control with Integral Backstepping Synthesized Method for Autonomous Ground Vehicle Control

Hamid Taghavifar [1,*] and Ardashir Mohammadzadeh [2]

[1] Department of Mechanical, Industrial and Aerospace Engineering, Concordia University, Montreal, QC H3G 1M8, Canada
[2] Multidisciplinary Center for Infrastructure Engineering, Shenyang University of Technology, Shenyang 110044 , China; a.mzadeh@sut.edu.cn
* Correspondence: hamid.taghavifar@concordia.ca; Tel.: +1-514-848-2424

Abstract: Autonomous ground vehicles (AGVs) operating in complex environments face the challenge of accurately following desired paths while accounting for uncertainties, external disturbances, and initial conditions, necessitating robust and adaptive control strategies. This paper addresses the critical path-tracking task in AGVs through a novel control framework for multilevel speed AGVs, considering both structured and unstructured uncertainties. The control system introduced in this study utilizes a nonlinear adaptive approach by integrating integral backstepping with terminal sliding mode control (IBTSMC). By incorporating integral action, IBTSMC continuously adjusts the control input to minimize tracking errors, improving tracking performance. The hybridization of the terminal sliding mode method enables finite time convergence, robustness, and a chatter-free response with reduced sensitivity to initial conditions. Furthermore, adaptive control compensators are developed to ensure robustness against unknown but bounded external disturbances. The Lyapunov stability theorem is employed to guarantee the global asymptotic stability of the closed-loop system and the convergence of tracking errors to the origin within finite time. To validate the effectiveness of the proposed control scheme, high-fidelity cosimulations are conducted using CarSim and MATLAB. Comparative analysis is performed with other methods reported in the literature. The results confirm that the proposed controller demonstrates competitive effectiveness in path-tracking tasks and exhibits strong efficiency under various road conditions, parametric uncertainties, and unknown disturbances.

Keywords: autonomous vehicles; backstepping; sliding mode; adaptive control

Citation: Taghavifar, H.; Mohammadzadeh, A. Adaptive Robust Terminal Sliding Mode Control with Integral Backstepping Synthesized Method for Autonomous Ground Vehicle Control. *Vehicles* **2023**, *5*, 1013–1029. https://doi.org/10.3390/vehicles5030055

Academic Editor: Chao Huang

Received: 19 July 2023
Revised: 10 August 2023
Accepted: 19 August 2023
Published: 21 August 2023

1. Introduction

1.1. Research Gap and Motivation

The fundamental objectives of future intelligent transportation systems revolve around optimizing traffic flow, ensuring improved driving safety, enhancing human comfort, maximizing transport efficiency, and minimizing road accidents [1,2]. Such goals strongly depend on the seamless integration of self-driving vehicles in multilevel traffic environments while demonstrating capabilities of safe and reliable route planning, traffic decision making, perception of complex environments, and navigation towards predefined destinations [3,4]. Recent technological progress in AI, as well as in software tools and hardware systems, has considerably contributed to the growing interest in the development of path-planning methods, sensing systems, and decision-making algorithms for autonomous systems [5]. While substantial attempts have been made to enhance the safety and efficacy of driverless cars, certain barriers remain, primarily because of the complex response of various vehicular components, input saturation (e.g., tire force saturation), other unmodeled dynamics, external disturbances, structural nonlinearities, and uncertainties concerned

with modeling parameters. Such challenges serve as the underpinning reasons for our much-needed studies to improve on existing control systems in terms of performance, robustness, reliability, and simplicity in design for the purpose of lane keeping or path-tracking performance [6,7]. Therefore, it is increasingly crucial to develop a comprehensive control system that can adapt to a wide range of operating conditions, regardless of the complexities embedded in the vehicle design. The ability to consistently ensure accurate lane keeping and precise path tracking in autonomous vehicles, especially in challenging driving situations, can successfully achieve this goal and considerably improve user satisfaction and the widespread adoption of self-driving cars [8].

The inherent limitations in the development of comprehensive algorithms and the adaptability of control strategies are two main obstacles in the deployment of path-following control systems. In order to address these challenges, a range of control methods has been proposed, including active front wheel steering (AFS), direct yaw moment control (DYC), and their hybrid combinations [9]. Although AFS and DYC have their respective advantages, such as simpler design and reduced control effort, it is well known that combined controllers can yield enhanced efficiency, improved performance, and increased stability during critical maneuvers [10]. AFS is frequently utilized to rectify undesirable handling characteristics, specifically addressing issues related to the vehicle's tendency to either understeer or oversteer. This is achieved by applying steering force specifically to the front wheels, enabling better control and stability during maneuvering [11]. However, AFS encounters certain limitations in attaining accurate path tracking, especially in demanding scenarios involving front steering saturation, speedy maneuvers, and abrupt turns [12]. Conversely, DYC offers a promising solution for improving dynamic orientation and heading angle, especially under demanding driving conditions. By generating an additional yaw moment through the application of brakes, DYC enhances the vehicle's maneuverability and stability, contributing to better control and responsiveness when faced with challenging circumstances [13]. In order to achieve precise path tracking, particularly under challenging driving conditions, the integration of a coordinated control strategy that combine AFS and DYC (AFS + DYC) has proven to be effective and reliable. Such integrated control schemes ensure that the desired trajectory is accurately followed, even in demanding driving scenarios, enhancing both the effectiveness and dependability of the path-tracking system [8]. These integrated control schemes provide a substantial boost to safety measures and instill a heightened sense of assurance when it comes to accomplishing precise path-tracking goals.

In order to achieve satisfactory lane-keeping performance, it is imperative to stabilize lateral displacement and minimize deviations in vehicle angle from the desired state [14]. A robust path-tracking control scheme should focus on minimizing the convergence of errors to negligible levels, ensuring precise and accurate tracking of the desired trajectory despite uncertainties and disturbances [15]. This necessity becomes especially crucial during dynamic situations, such as navigating on twisty roads with reduced grip, executing sudden critical maneuvers, driving on slippery surfaces, or facing scenarios that require a desired yaw rate. Under such conditions, the preference lies with robust adaptive control approaches, which possess the ability to effectively handle unknown dynamics; generate control efforts according to the required demand; and guarantee overall system safety, security, and stability in achieving optimal path-tracking performance [4].

1.2. Literature Review

Extensive research investigations have focused on path-tracking control for road vehicles, aiming to develop a diverse range of robust control algorithms. These encompass the implementation of sliding-mode controller (SMC) techniques [16], the utilization of neural networks [17,18], integration of fuzzy systems (FLS) [19,20], adoption of backstepping methodologies [21], and exploration of various optimal and model-predictive control approaches [22]. In particular, SMC has been successfully employed for the chassis control of four-wheel independent control electric vehicles [23], as well as for hierarchical energy

efficiency optimization control strategies in distributed drive electric vehicles [24]. These studies contribute to the ongoing exploration of effective and adaptable control strategies precise path tracking in diverse driving scenarios. For example, in [22], a controller design approach was proposed for path tracking of autonomous ground vehicles using multi-constraint nonlinear predictive control (NMPC) to improve transient performance and consider rollover prevention. The proposed method incorporated a neural network autoregressive model, Frenet–Serret differential geometry-based path following, and vehicle vertical motion modeling in order to accomplish enhanced yaw stabilization and transient tracking performance while considering input saturation. In [20], a robust fuzzy control approach was presented for lateral path following of autonomous road vehicles subject to parametric uncertainties, disturbances, and varying speeds. The proposed method utilized a non-singleton fuzzy system to account for parametric variations and errors related to measurements to guarantee path-following performance under diverse operating conditions and external disturbances. In [25], a high-performance automatic steering control strategy was developed for AGVs by establishing a vehicle–road system model and proposing automatic a steering control algorithm based on a backstepping sliding mode variable structure control. The study demonstrated improved system dynamics, robustness against vehicular velocity, real-time performance, and tracking accuracy.

1.3. Contribution and Paper Organization

By reviewing the existing literature, it can be inferred that the path-tracking control of autonomous vehicles poses challenges due to the nonlinear and complex dynamics of the vehicle, as well as the uncertainties associated with tire–road forces. These factors contribute to the overall complexity of the system dynamics, making path tracking control more difficult. Previous studies have proposed coordinated control architectures that combine active front wheel steering (AFS) and direct yaw moment control (DYC), commonly referred to as AFS+DYC. These coordinated control methods have demonstrated promising results in achieving accurate and safe path-tracking performance. Through the integration of both AFS and DYC, these methods significantly enhance the overall performance and reliability of the path-tracking control system.Therefore, this paper makes several key contributions, which can be summarized as follows:

- An integral backstepping control method is hybridized with a terminal sliding mode control method to enhance the lateral path-tracking performance of AGVs;
- A novel disturbance observer is designed to handle unknown but bounded disturbances, and a controller compensator is devised based on an adaptive disturbance observer and unknown weight approximations;
- High-fidelity cosimulations are conducted using CarSim, and MATLAB is utilized to verify the effectiveness of the proposed controller in terms of stabilizing tracking errors and robustness against parametric uncertainties and external disturbances.

2. Problem Formulation

In this study, a widely utilized two-degrees-of-freedom bicycle model is employed. This model assumes a flat road surface and symmetry between the right and left tracks of the vehicle. Furthermore, it takes into account the minimal compliance of the chassis and suspension system components, disregarding their response to minor road irregularities, and no pitch and roll motion due to aerodynamic forces. By considering these factors, with this study, we aim to accurately capture the essential dynamics of the vehicle for analysis and development of control strategies.

Furthermore, negligible variations in longitudinal forces are typically assumed when the travel speed remains constant. However, it is crucial to highlight that an adequate forward speed is required to produce lateral forces in relation to the slip angles during cornering maneuvers. Consequently, the complexities of longitudinal dynamics can be disregarded, simplifying the three degrees of freedom in the plane of motion into a conventional bicycle model. By focusing on two primary modes of motion derived from the

vehicle dynamics discussed herein, the desired path-tracking dynamics can be expressed (Figure 1).

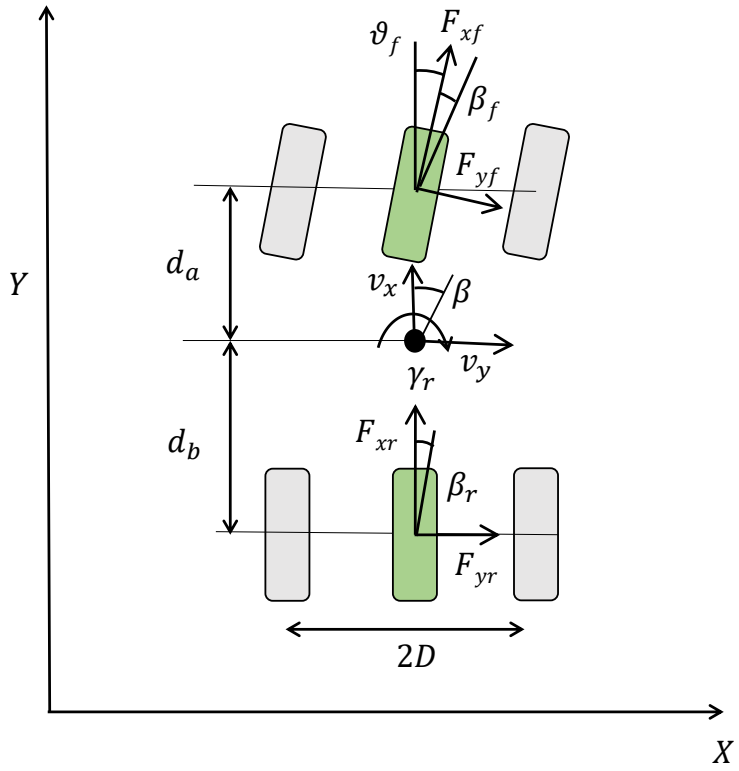

Figure 1. Yaw-plane two-DoF model.

It is essential for the vehicle's yaw angle to converge to the desired state within a limited time period in order to ensure yaw stability. This convergence allows for better control and stability during the vehicle's rotational motion. Additionally, minimizing the lateral offset of the vehicle by reducing its lateral position plays a crucial role in effective lane-keeping performance, thus enhancing overall safety. The lateral displacement error denotes the minimum distance between the vehicle and the intended trajectory, quantified through an orthogonal projection. Consequently, in this study, the path-tracking control approach is based on the utilization of a bicycle model. This model serves as a simplified representation of the vehicle's dynamics, enabling a comprehensive analysis of its behavior with respect to steering and lateral movements. By employing this model, a deeper understanding of the vehicle's response and control can be attained, facilitating effective path-tracking strategies [26].

$$\begin{aligned} m\left(v_x\gamma_r + \dot{v}_y\right) &= \sum_i F_{yi} \quad i = f, r \\ I_{zz}\dot{\gamma}_r &= \sum M = F_{yf}d_a - F_{yr}d_b + \Delta M \end{aligned} \tag{1}$$

In the provided bicycle model, the lateral forces exerted by the front and rear tires are denoted as F_{yf} and F_{yr}, respectively. The variables m and I_{zz} represent the vehicle's mass and moment of inertia about the yaw axis, respectively. The front and rear wheelbase components are indicated by d_a and d_b, respectively. The vehicle's traveling speed is represented by v_x, while γ_r signifies the chassis yaw rate, and v_y denotes the lateral velocity of the vehicle. Additionally, the direct yaw moment applied to the vehicle, denoted as ΔM, can be expressed as follows:

$$\Delta M = \sum_j \sum_i F_{xij} D(-1)^i \quad i = f, r; j = r, l \tag{2}$$

In the proposed system, the tires are distinguished by subscript i, where r and l denote the right and left track tires respectively, while subscripts j with f and r represent the front and rear tires, respectively. To effectively distribute the controller-generated direct yaw control (DYC) among the four tires, an optimal policy can be employed, taking into consideration the vehicle's wheelbase components, which are denoted as d_a and d_b. This distribution of DYC ensures balanced handling and control throughout the vehicle. Furthermore, adhering to the assumptions made for the two-degrees-of-freedom (two-DoF) bicycle model, the DYC is evenly divided between the right and left tire tracks, allowing for precise and responsive steering performance. The correlation between the tire sideslip angles and the lateral forces produced by the tires can be approximated as proportional, where the specific proportionality is dictated by the cornering stiffness parameters. This relationship signifies that changes in the sideslip angles directly influence the magnitude of lateral forces generated by the tires. By understanding and considering this proportional connection, it becomes possible to effectively control and manipulate the vehicle's lateral dynamics during cornering maneuvers.

$$F_{yi} = c_i \beta_i \,, \quad c_i = \hat{c}_i + \delta \hat{c}_i \quad i = f, r \tag{3}$$

where $\delta \hat{c}_i$ accounts for the deviations from the nominal value of the tire cornering stiffness due to modeling uncertainties. These uncertain parameters capture the bounded uncertainties that arise beyond the linear deflection region and near the tire's saturation point. Consequently, the expressions for the sideslip angles regarding the front and rear axle tires can be formulated as follows:

$$\beta_f + \vartheta_f = atan\left(\frac{v_x \sin\left(atan\left(\frac{v_y}{v_x}\right)\right) + \gamma_r d_a}{v_x \cos\left(atan\left(\frac{v_y}{v_x}\right)\right)}\right) \tag{4}$$

$$\beta_r = atan\left(\frac{v_x \sin\left(atan\left(\frac{v_y}{v_x}\right)\right) - \gamma_r d_b}{v_x \cos\left(atan\left(\frac{v_y}{v_x}\right)\right)}\right) \tag{5}$$

The vehicle's sideslip angle can be defined as the ratio of the lateral velocity component to the longitudinal velocity component, represented as $atan\left(\frac{v_y}{v_x}\right)$. Here, ϑ_f denotes the front wheel steering angle, and β_f and β_r represent the tire slip angles for the front and rear axles, respectively. By substituting Equations (2) and (5) into Equation (1), the governing equations can be effectively reformulated as follows:

$$\begin{aligned} \dot{v}_y = {} & \frac{c_f}{m}\left\{atan\left(\frac{v_x \sin\left(atan\left(\frac{v_y}{v_x}\right)\right) + \gamma_r d_a}{v_x \cos\left(atan\left(\frac{v_y}{v_x}\right)\right)}\right) - \vartheta_f\right\} + \\ & \frac{c_r}{m}\left\{atan\left(\frac{v_x \sin\left(atan\left(\frac{v_y}{v_x}\right)\right) - \gamma_r d_b}{v_x \cos\left(atan\left(\frac{v_y}{v_x}\right)\right)}\right)\right\} - v_x \gamma_r \end{aligned} \tag{6}$$

$$\begin{aligned} \dot{\gamma}_r = {} & \frac{c_f d_a}{I_{zz}}\left\{atan\left(\frac{v_x \sin\left(atan\left(\frac{v_y}{v_x}\right)\right) + \gamma_r d_a}{v_x \cos\left(atan\left(\frac{v_y}{v_x}\right)\right)}\right) - \vartheta_f\right\} - \\ & \frac{c_f d_b}{I_{zz}}\left\{atan\left(\frac{v_x \sin\left(atan\left(\frac{v_y}{v_x}\right)\right) - \gamma_r d_b}{v_x \cos\left(atan\left(\frac{v_y}{v_x}\right)\right)}\right)\right\} + \frac{\Delta M}{I_{zz}} \end{aligned} \tag{7}$$

In light of the aforementioned dynamics, the governing equations of the system can be reformulated as follows:

$$\begin{aligned}\dot{\eta}_1(t) &= \mathcal{F}_1\left(\underline{\eta}(t)\right) + \mathcal{G}_1\left(\underline{\eta}(t)(t)\right)\theta_1(t)\\ \dot{\eta}_2(t) &= \mathcal{F}_2\left(\underline{\eta}(t)\right) + \mathcal{G}_2\left(\underline{\eta}(t)(t)\right)\theta_2(t)\end{aligned} \tag{8}$$

where $\underline{\eta}(t) = \begin{bmatrix} v_y & \gamma_r \end{bmatrix}$, $\mathcal{G}_1\left(\underline{\eta}(t)\right) = -\frac{c_f}{m}$, $\mathcal{G}_2\left(\underline{x}(t)\right) = \frac{1}{I_{zz}}$, $\theta_1(t) = \vartheta_f$, $\theta_2(t) = \Delta M$, and the following scalar functions are introduced as:

$$\begin{aligned}\mathcal{F}_1\left(\underline{\eta}(t)\right) = \frac{c_f}{m}\left\{atan\left(\frac{v_x \sin\left(atan\left(\frac{v_y}{v_x}\right)\right) + \gamma_r d_a}{v_x \cos\left(atan\left(\frac{v_y}{v_x}\right)\right)}\right)\right\} +\\ \frac{c_r}{m}\left\{atan\left(\frac{v_x \sin\left(atan\left(\frac{v_y}{v_x}\right)\right) - \gamma_r d_b}{v_x \cos\left(atan\left(\frac{v_y}{v_x}\right)\right)}\right)\right\} - v_x\gamma_r\end{aligned} \tag{9}$$

$$\begin{aligned}\mathcal{F}_2\left(\underline{\eta}(t)\right) = \frac{c_f d_a}{I_{zz}}\left\{atan\left(\frac{v_x \sin\left(atan\left(\frac{v_y}{v_x}\right)\right) + \gamma_r d_a}{v_x \cos\left(atan\left(\frac{v_y}{v_x}\right)\right)}\right)\right\} -\\ \frac{c_f d_b}{I_{zz}}\left\{atan\left(\frac{v_x \sin\left(atan\left(\frac{v_y}{v_x}\right)\right) - \gamma_r d_b}{v_x \cos\left(atan\left(\frac{v_y}{v_x}\right)\right)}\right)\right\}\end{aligned} \tag{10}$$

3. Main Results

3.1. Design of Integral Backstepping with Terminal Sliding Mode Controller

In this section, the development of an integral backstepping controller is presented for path-following control of autonomous road vehicles. Integral backstepping controllers provide several advantages in control applications. They enhance tracking performance by effectively addressing steady-state tracking errors through integral action. These controllers are robust to model uncertainties, disturbances, and parameter variations, ensuring reliable performance under varying operating conditions. They also reduce sensitivity to disturbances and compensate for persistent disturbances and external forces. Integral backstepping controllers mitigate steady-state errors, leading to precise regulation of system output. Additionally, they offer versatility across control applications, making them suitable for a wide range of engineering and control scenarios.

To achieve improved tracking performance through the integral backstepping controller, the system governing equations in Equation (8) can be reformulated as:

$$\begin{aligned}\dot{\eta}_1(t) &= \mathcal{F}_1\left(\underline{\eta}(t)\right) + \mathcal{G}_1\left(\underline{\eta}(t)\right)\xi_1(t)\\ \dot{\xi}_1(t) &= \mathcal{U}_1(t)\end{aligned} \tag{11}$$

$$\begin{aligned}\dot{\eta}_2(t) &= \mathcal{F}_2\left(\underline{\eta}(t)\right) + \mathcal{G}_2\left(\underline{\eta}(t)\right)\xi_2(t)\\ \dot{\xi}_2(t) &= \mathcal{U}_2(t)\end{aligned} \tag{12}$$

where $\theta_1(t)$ and $\theta_1(t)$ are replaced by ξ_1 and ξ_2, respectively, as the virtual controllers, and $\mathcal{U}_1$ and $\mathcal{U}_2$ represent the new control inputs.

Theorem 1. *For the system dynamics for the autonomous ground vehicle (AGV) expressed in Equations (11) and (12), an integral backstepping with terminal sliding mode controller (IBTSMC) can be designed with global asymptotic stability.*

Proof of Theorem 1. By defining $e_1 = \eta_1 - \eta_{1d}$ and $e_2 = \eta_2 - \eta_{2d}$ as the tracking errors for the system, a terminal sliding mode controller is developed because of the several benefits it offers, including rapid convergence, robustness, and avoidance of singularities. To achieve these advantages, we adopt a non-singular terminal sliding surface approach:

$$s_1 = e_1 + \varpi_1 \int_0^t (e_1(\rho))^{q/p} d\rho \tag{13}$$

$$s_2 = e_2 + \varpi_2 \int_0^t (e_2(\rho))^{q/p} d\rho \tag{14}$$

where $\varpi, p, q \in R^+$ and $1 < \frac{p}{q} < 2$; and p and q are odd numbers. Given the time derivative of the sliding surfaces:

$$\dot{s}_1 = \dot{e}_1 + \varpi_1 e_1^{q/p}(t) + \frac{\varpi_1 q}{p} \int_0^t (e_1(\rho))^{q-p/p} d\rho \tag{15}$$

$$\dot{s}_2 = \dot{e}_2 + \varpi_2 e_2^{q/p}(t) + \frac{\varpi_2 q}{p} \int_0^t (e_2(\rho))^{q-p/p} d\rho \tag{16}$$

Let us create a Lyapunov candidate function as:

$$\mathcal{V}_1(s_i, t) = \frac{1}{2} \sum_{i=1}^{2} s_i^2 \tag{17}$$

Taking the time derivative of Equation (17) yields:

$$\dot{\mathcal{V}}_1(s_i) = \frac{\partial \mathcal{V}_1(s_i)}{\partial s_i} \frac{\partial s_i}{\partial t} = \frac{\partial \mathcal{V}_1}{\partial s_1} \begin{bmatrix} \mathcal{F}_1\left(\underline{\eta}(t)\right) + \mathcal{G}_1\left(\underline{\eta}(t)\right)\xi_1(t) + \varpi_1 e_1^{q/p}(t) + \\ \frac{\varpi_1 q}{p} \int_0^t (e_1(\rho))^{q-p/p} d\rho - \dot{\eta}_{1d} \end{bmatrix} + \tag{18}$$

$$\frac{\partial \mathcal{V}_1}{\partial s_2} \left[\mathcal{F}_2\left(\underline{\eta}(t)\right) + \mathcal{G}_2\left(\underline{\eta}(t)\right)\xi_2(t) + \varpi_2 e_2^{q/p}(t) + \frac{\varpi_2 q}{p} \int_0^t (e_2(\rho))^{q-p/p} d\rho - \dot{\eta}_{2d} \right]$$

Let us assume that there exists $\xi_1 = \Omega_1\left(\underline{\eta}\right)$ and $\xi_2 = \Omega_2\left(\underline{\eta}\right)$ such that:

$$\frac{\partial \mathcal{V}_1}{\partial s_1} \left[\mathcal{F}_1\left(\underline{\eta}(t)\right) + \mathcal{G}_1\left(\underline{\eta}(t)\right)\xi_1(t) + \varpi_1 e_1^{q/p}(t) + \frac{\varpi_1 q}{p} \int_0^t (e_1(\rho))^{q-p/p} d\rho - \dot{\eta}_{1d} \right] \leqslant -\psi_1(s_1) \tag{19}$$

and

$$\frac{\partial \mathcal{V}_1}{\partial s_2} \left[\mathcal{F}_2\left(\underline{\eta}(t)\right) + \mathcal{G}_2\left(\underline{\eta}(t)\right)\xi_2(t) + \varpi_2 e_2^{q/p}(t) + \frac{\varpi_2 q}{p} \int_0^t (e_2(\rho))^{q-p/p} d\rho - \dot{\eta}_{2d} \right] \leqslant -\psi_2(s_2) \tag{20}$$

where $\psi_1(s_1)$ and $\psi_2(s_2)$ are positive definite functions. Thus,

$$\dot{\mathcal{V}}_1(s_i) \leqslant -\psi_1(s_1) - \psi_2(s_2) \leqslant -\psi_3(s_1, s_2) \tag{21}$$

Thus, the stability proof of the closed-loop system can be completed, given the virtual control signals. Now, let us define two new variables as $\zeta_1 = \xi_1 - \Omega_1\left(\underline{\eta}\right)$ and $\zeta_2 = \xi_2 - \Omega_2\left(\underline{\eta}\right)$.

Given the time derivative of Equation (21):

$$\begin{aligned} \dot{\zeta}_1 &= \mathcal{U}_1 - \dot{\Omega}_1\left(\underline{\eta}\right) \\ \dot{\zeta}_2 &= \mathcal{U}_2 - \dot{\Omega}_2\left(\underline{\eta}\right) \end{aligned} \tag{22}$$

Using some mathematical manipulations, the tracking error dynamics can be written as:

$$\dot{e}_i = \mathcal{F}_i\left(\underline{\eta}(t)\right) + \mathcal{G}_i\left(\underline{\eta}(t)\right)\zeta_i(t) + \mathcal{G}_i\left(\underline{\eta}(t)\right)\Omega_i\left(\underline{\eta}\right) - \dot{\eta}_{id} \quad i = 1, 2 \tag{23}$$

Now, let us construct a Lyapunov candidate function as:

$$\mathcal{V}_2(s_i, \zeta_i) = \frac{1}{2}\sum_{i=1}^{2}\left(s_i^2 + \zeta_i^2\right) \tag{24}$$

The time derivative of Equation (24) becomes:

$$\begin{aligned} \dot{\mathcal{V}}_2(s_i, \zeta_i) = \frac{\partial \mathcal{V}_2(s_i)}{\partial s_i}\frac{\partial s_i}{\partial t} + \frac{\partial \mathcal{V}_2(\zeta_i)}{\partial \zeta_i}\frac{\partial \zeta_i}{\partial t} = \frac{\partial \mathcal{V}_1}{\partial s_1}\begin{bmatrix} \mathcal{F}_1\left(\underline{\eta}(t)\right) + \mathcal{G}_1\left(\underline{\eta}(t)\right)\zeta_1(t) \\ +\mathcal{G}_1\left(\underline{\eta}(t)\right)\Omega_1\left(\underline{\eta}\right) + \omega_1 e_1^{q/p}(t) + \\ \frac{\omega_1 q}{p}\int_0^t \left(e_1(\rho)\right)^{q-p/p} d\rho - \dot{\eta}_{1d} \end{bmatrix} \\ + \frac{\partial \mathcal{V}_2}{\partial s_2}\begin{bmatrix} \mathcal{F}_2\left(\underline{\eta}(t)\right) + \mathcal{G}_2\left(\underline{\eta}(t)\right)\zeta_2(t) + \mathcal{G}_2\left(\underline{\eta}(t)\right)\Omega_2\left(\underline{\eta}\right) + \omega_2 e_2^{q/p}(t) + \\ \frac{\omega_2 q}{p}\int_0^t \left(e_2(\rho)\right)^{q-p/p} d\rho - \dot{\eta}_{2d} \end{bmatrix} + \\ \frac{\partial \mathcal{V}_2(\zeta_1)}{\partial \zeta_1}\left(\mathcal{U}_1 - \dot{\Omega}_1\left(\underline{\eta}\right)\right) + \frac{\partial \mathcal{V}_2(\zeta_2)}{\partial \zeta_2}\left(\mathcal{U}_2 - \dot{\Omega}_2\left(\underline{\eta}\right)\right) \end{aligned} \tag{25}$$

The system can be further rearranged as:

$$\begin{aligned} \dot{\mathcal{V}}_2(s_i, \zeta_i) \leqslant -\psi_3(s_1, s_1) + \frac{\partial \mathcal{V}_2}{\partial s_1}\left[\mathcal{G}_1\left(\underline{\eta}(t)\right)\zeta_1(t)\right] + \frac{\partial \mathcal{V}_2}{\partial s_2}\left[\mathcal{G}_2\left(\underline{\eta}(t)\right)\zeta_2(t)\right] + \\ \frac{\partial \mathcal{V}_2(\zeta_1)}{\partial \zeta_1}\left(\mathcal{U}_1 - \dot{\Omega}_1\left(\underline{\eta}\right)\right) + \frac{\partial \mathcal{V}_2(\zeta_2)}{\partial \zeta_2}\left(\mathcal{U}_2 - \dot{\Omega}_2\left(\underline{\eta}\right)\right) \end{aligned} \tag{26}$$

By using some mathematical manipulations, Equation (26) can be rewritten as:

$$\begin{aligned} \dot{\mathcal{V}}_2(s_i, \zeta_i) \leqslant -\psi_3(s_1, s_1) + \frac{\partial \mathcal{V}_2}{\partial s_1}\left[\mathcal{G}_1\left(\underline{\eta}(t)\right)\zeta_1(t)\right] + \frac{\partial \mathcal{V}_2}{\partial s_2}\left[\mathcal{G}_2\left(\underline{\eta}(t)\right)\zeta_2(t)\right] + \\ \zeta_1(t)\left(\mathcal{U}_1 - \dot{\Omega}_1\left(\underline{\eta}\right)\right) + \zeta_2(t)\left(\mathcal{U}_2 - \dot{\Omega}_1\left(\underline{\eta}\right)\right) \end{aligned} \tag{27}$$

$$\dot{\mathcal{V}}_2(s_i,\zeta_i) \leqslant -\psi_3(s_1,s_1) + \zeta_1(t)\left(\frac{\partial \mathcal{V}_2}{\partial s_1}\mathcal{G}_1\left(\underline{\eta}(t)\right)\mathcal{U}_1 - \dot{\Omega}_1\left(\underline{\eta}\right)\right) + \zeta_2(t)\left(\frac{\partial \mathcal{V}_2}{\partial s_2}\mathcal{G}_2\left(\underline{\eta}(t)\right)\mathcal{U}_2 - \dot{\Omega}_2\left(\underline{\eta}\right)\right) \tag{28}$$

Finally, by defining the control inputs as:

$$\begin{aligned}\mathcal{U}_1 &= \left[\frac{\partial \mathcal{V}_1}{\partial s_1}\mathcal{G}_1\left(\underline{\eta}(t)(t)\right)\right]^{-1}\dot{\Omega}_2\left(\underline{\eta}(t)\right)\\ \mathcal{U}_2 &= \left[\frac{\partial \mathcal{V}_2}{\partial s_2}\mathcal{G}_2\left(\underline{\eta}(t)(t)\right)\right]^{-1}\dot{\Omega}_2\left(\underline{\eta}(t)\right)\end{aligned} \tag{29}$$

Equation (28) reduces to $\dot{\mathcal{V}}_2(s_i,\zeta_i) - \leqslant \psi_3(s_1,s_1)$, which completes the stability proof. □

3.2. Adaptive Robustness Against External Disturbances

The sources of external disturbance in path-tracking for autonomous vehicles can stem from various factors. These sources may include unpredictable weather conditions, such as strong winds, rain, or snow, which can affect the vehicle's handling and stability. Road conditions, such as uneven surfaces, potholes, or debris on the road, can introduce disturbances that impact the vehicle's trajectory. The effect of external disturbances can be incorporated in the system dynamics of Equation (8) as:

$$\begin{aligned}\dot{\eta}_1(t) &= \mathcal{F}_1\left(\underline{\eta}(t)\right) + \mathcal{G}_1\left(\underline{\eta}(t)\right)\xi_1(t) + \phi_1\left(\underline{\eta}(t)\right)\\ \dot{\xi}_1(t) &= U_1(t)\end{aligned} \tag{30}$$

$$\begin{aligned}\dot{\eta}_2(t) &= \mathcal{F}_2\left(\underline{\eta}(t)\right) + \mathcal{G}_2\left(\underline{\eta}(t)\right)\xi_2(t) + \phi_2\left(\underline{\eta}(t)\right)\\ \dot{\xi}_2(t) &= U_2(t)\end{aligned} \tag{31}$$

where $\phi_1\left(\underline{\eta}(t)\right)$ and $\phi_2\left(\underline{\eta}(t)\right)$ are bounded but unknown disturbances applied to the AGV system dynamics.

$$\begin{aligned}\dot{\eta}_1(t) &= \mathcal{F}_1\left(\underline{\eta}(t)\right) + \mathcal{G}_1\left(\underline{\eta}(t)\right)\xi_1(t) + W_1^T\sigma\left(\underline{\eta}(t)\right)\\ \dot{\xi}_1(t) &= U_1(t)\\ \dot{\eta}_2(t) &= \mathcal{F}_2\left(\underline{\eta}(t)\right) + \mathcal{G}_2\left(\underline{\eta}(t)\right)\xi_2(t) + W_1^T\sigma\left(\underline{\eta}(t)\right)\\ \dot{\xi}_2(t) &= U_2(t)\end{aligned} \tag{32}$$

where $W_1, W_2 \in \mathcal{R}^{n\times s}$ represent the unknown weight matrices, and $\phi_1\left(\underline{\eta}\right) = \left[\phi_1^1\left(\underline{\eta}\right), \phi_1^2\left(\underline{\eta}\right), ..., \phi_1^s\left(\underline{\eta}\right)\right]^T$ and $\phi_2\left(\underline{\eta}\right) = \left[\phi_2^1\left(\underline{\eta}\right), \phi_2^2\left(\underline{\eta}\right), ..., \phi_2^s\left(\underline{\eta}\right)\right]^T$ are global Lipschits functions acting as the base functions with $\phi_1\left(\underline{\eta}\right), \phi_1\left(\underline{\eta}\right) : \mathcal{R}^n \to \mathcal{R}^s$.

Theorem 2. *For the system dynamics for the autonomous ground vehicle (AGV) expressed in Equations (8) and (33), an integral backstepping with terminal sliding mode controller (IBTSMC) can be designed with global asymptotic stability, and the adaptation laws are derived as:*

$$\begin{aligned}\dot{\hat{W}}_1 &= \Gamma_1^{-1}\sigma\left(\underline{\eta}(t)\right)s_1\\ \dot{\hat{W}}_2 &= \Gamma_2^{-1}\sigma\left(\underline{\eta}(t)\right)s_2\end{aligned} \tag{33}$$

with the following control compensators:

$$\begin{aligned} u_1^c &= \left[\mathcal{G}_1\left(\underline{\eta}(t)\right)\right]^{-1}\hat{W}_1^T\sigma\left(\underline{\eta}(t)\right) \\ u_2^c &= \left[\mathcal{G}_2\left(\underline{\eta}(t)\right)\right]^{-1}\hat{W}_2^T\sigma\left(\underline{\eta}(t)\right) \end{aligned} \tag{34}$$

Proof of Theorem 2. By defining $\xi_1(t) = \Omega_1\left(\underline{\eta}\right) + u_1^c + \zeta_1(t)$ and $\xi_2(t) = \Omega_2\left(\underline{\eta}\right) + u_2^c + \zeta_2(t)$, the system dynamics in Equation (33) can be rewritten as:

$$\begin{aligned} \dot{\eta}_1(t) &= \mathcal{F}_1\left(\underline{\eta}(t)\right) + \mathcal{G}_1\left(\underline{\eta}(t)\right)\left[\Omega_1\left(\underline{\eta}\right) + u_1^c + \zeta_1(t)\right] + W_1^T\sigma\left(\underline{\eta}(t)\right) \\ \dot{\xi}_1(t) &= U_1(t) \\ \dot{\eta}_2(t) &= \mathcal{F}_2\left(\underline{\eta}(t)\right) + \mathcal{G}_2\left(\underline{\eta}(t)\right)\left[\Omega_2\left(\underline{\eta}\right) + u_2^c + \zeta_2(t)\right] + W_1^T\sigma\left(\underline{\eta}(t)\right) \\ \dot{\xi}_2(t) &= U_2(t) \end{aligned} \tag{35}$$

where u_1^c and u_2^c are the control compensation signals. Under the new system dynamics, $\dot{s}_1$ and $\dot{s}_2$ can be expressed as:

$$\begin{aligned} \dot{s}_1 = \mathcal{F}_1\left(\underline{\eta}(t)\right) + \mathcal{G}_1\left(\underline{\eta}(t)\right)\zeta_1(t) + \mathcal{G}_1\left(\underline{\eta}(t)\right)\Omega_1\left(\underline{\eta}\right) + \omega_1 e_1^{q/p}(t) + \\ \frac{\omega_1 q}{p}\int_0^t (e_1(\rho))^{q-p/p}d\rho - \dot{\eta}_{1d} + \mathcal{G}_1\left(\underline{\eta}(t)\right)u_1^c + W_1^T\sigma\left(\underline{\eta}(t)\right) \end{aligned} \tag{36}$$

$$\begin{aligned} \dot{s}_2 = \mathcal{F}_2\left(\underline{\eta}(t)\right) + \mathcal{G}_2\left(\underline{\eta}(t)\right)\zeta_2(t) + \mathcal{G}_2\left(\underline{\eta}(t)\right)\Omega_2\left(\underline{\eta}\right) + \omega_2 e_2^{q/p}(t) + \\ \frac{\omega_2 q}{p}\int_0^t (e_2(\rho))^{q-p/p}d\rho - \dot{\eta}_{2d} + \mathcal{G}_2\left(\underline{\eta}(t)\right)u_2^c + W_2^T\sigma\left(\underline{\eta}(t)\right) \end{aligned} \tag{37}$$

Additionally, it is assumed that $\tilde{W}_1 = W_1 - \hat{W}_1$ and $\tilde{W}_2 = W_2 - \hat{W}_2$, where $\hat{W}_1$ and $\hat{W}_2$ are approximations of unknown weight matrices W_1 and W_2, respectively. Now, let us construct a new Lyapunov candidate function as:

$$\mathcal{V}_3(s_i, \zeta_i, \tilde{W}_1, \tilde{W}_2) = \frac{1}{2}\sum_{i=1}^{2}\left(s_i^2 + \zeta_i^2\right) + \frac{1}{2}\tilde{W}_1^T\Gamma_1^{-1}\tilde{W}_1 + \frac{1}{2}\tilde{W}_2^T\Gamma_2^{-1}\tilde{W}_2 \tag{38}$$

Given the time derivative of Equation (38), together with Equations (36) and (37), as well as the proof in Theorem 1, we have:

$$\begin{aligned} \dot{\mathcal{V}}_3(s_i, \zeta_i, \tilde{W}_1, \tilde{W}_2) &= \dot{s}_1 s_1 + \dot{s}_2 s_2 + \dot{\zeta}_1\zeta_1 + \dot{\zeta}_2\zeta_2 - \tilde{W}_1^T\Gamma_1^{-1}\dot{\hat{W}}_1 - \tilde{W}_2^T\Gamma_2^{-1}\dot{\hat{W}}_2 \\ &= s_1\left[\begin{array}{l} \mathcal{F}_1\left(\underline{\eta}(t)\right) + \mathcal{G}_1\left(\underline{\eta}(t)\right)\zeta_1(t) + \mathcal{G}_1\left(\underline{\eta}(t)\right)\Omega_1\left(\underline{\eta}\right) + \omega_1 e_1^{q/p}(t) + \\ \frac{\omega_1 q}{p}\int_0^t (e_1(\rho))^{q-p/p}d\rho - \dot{\eta}_{1d} + \mathcal{G}_1\left(\underline{\eta}(t)\right)u_1^c + W_1^T\sigma\left(\underline{\eta}(t)\right) \end{array}\right] \\ &+ s_2\left[\begin{array}{l} \mathcal{F}_2\left(\underline{\eta}(t)\right) + \mathcal{G}_2\left(\underline{\eta}(t)\right)\zeta_2(t) + \mathcal{G}_2\left(\underline{\eta}(t)\right)\Omega_2\left(\underline{\eta}\right) + \omega_2 e_2^{q/p}(t) + \\ \frac{\omega_2 q}{p}\int_0^t (e_2(\rho))^{q-p/p}d\rho - \dot{\eta}_{2d} + \mathcal{G}_2\left(\underline{\eta}(t)\right)u_2^c + W_2^T\sigma\left(\underline{\eta}(t)\right) \end{array}\right] + \\ &\zeta_1\left(\mathcal{U}_1 - \dot{\Omega}_1\left(\underline{\eta}\right)\right) + \zeta_2\left(\mathcal{U}_2 - \dot{\Omega}_1\left(\underline{\eta}\right)\right) - \tilde{W}_1^T\Gamma_1^{-1}\dot{\hat{W}}_1 - \tilde{W}_2^T\Gamma_2^{-1}\dot{\hat{W}}_2 \end{aligned} \tag{39}$$

By rearranging Equation (39) and using the result of Theorem 1:

$$\begin{aligned}\dot{\mathcal{V}}_3(s_i,\zeta_i,\tilde{W}_1,\tilde{W}_2) \leqslant -\psi_3(s_1,s_1)+s_1\mathcal{G}_1\left(\underline{\eta}(t)\right)u_1^c+s_1W_1^T\sigma\left(\underline{\eta}(t)\right)+\\ s_2\mathcal{G}_2\left(\underline{\eta}(t)\right)u_2^c+s_2W_2^T\sigma\left(\underline{\eta}(t)\right)-\tilde{W}_1^T\Gamma_1^{-1}\dot{\hat{W}}_1-\tilde{W}_2^T\Gamma_2^{-1}\dot{\hat{W}}_2\end{aligned} \tag{40}$$

By applying the compensator controllers signals in Equation (34), the system dynamics in Equation (41) can be expressed as:

$$\begin{aligned}\dot{\mathcal{V}}_3(s_i,\zeta_i,\tilde{W}_1,\tilde{W}_2) \leqslant -\psi_3(s_1,s_1)+s_1\tilde{W}_1^T\sigma\left(\underline{\eta}(t)\right)+s_2\tilde{W}_2^T\sigma\left(\underline{\eta}(t)\right)-\\ \tilde{W}_1^T\Gamma_1^{-1}\dot{\hat{W}}_1-\tilde{W}_2^T\Gamma_2^{-1}\dot{\hat{W}}_2\end{aligned} \tag{41}$$

By rearranging Equation (41), one can write:

$$\dot{\mathcal{V}}_3(s_i,\zeta_i,\tilde{W}_1,\tilde{W}_2) \leqslant -\psi_3(s_1,s_1)+\tilde{W}_1^T\left[\sigma\left(\underline{\eta}(t)\right)s_1-\Gamma_1^{-1}\dot{\hat{W}}_1\right]+\tilde{W}_2^T\left[\sigma\left(\underline{\eta}(t)\right)s_2-\Gamma_2^{-1}\dot{\hat{W}}_2\right] \tag{42}$$

Finally, by applying the adaptation laws derived in Equation (33), the time derivative of the function can be reduced as:

$$\dot{\mathcal{V}}_3(s_i,\zeta_i,\tilde{W}_1,\tilde{W}_2) \leqslant -\psi_3(s_1,s_1) \tag{43}$$

And since $\psi(s_1,S_2)$ is a positive definite function, the stability proof is complete. □

4. Discussion

A high-fidelity CarSim–Matlab simulation was conducted to validate the effectiveness of the proposed IBTSMC strategy. A schematic diagram of the simulation is shown in Figure 2. Table 1 provides the simulation parameters used in this study. In this study, the assumption was that the car is traveling on a dry road, preventing any sideways sliding. This section evaluates the performance of the designed controller under different operating conditions. The performance of the proposed controller in this study is compared to a benchmarking robust backstepping super-twisting sliding mode control (BSSTSMC) [27]. Reference trajectories η_{1d} and η_{2d} are expressed as follows [22]:

$$\begin{aligned}\eta_{1d} &= \tfrac{d}{dt}\tan^{-1}\left\{0.5\left(\tfrac{1}{\cosh(\bar{p})}\right)^2-0.31\left(\tfrac{1}{\cosh(\bar{q})}\right)^2\right\}\\ \eta_{2d} &= \tfrac{d}{dt}\{2.01(1+\tanh(\bar{p}))-2.85(1+\tanh(\bar{q}))\}\\ \bar{p} &= -1.2+2.3(v_xt-27.2)/25\\ \bar{q} &= -1.2+2.3(v_xt-56.45)/21.94\end{aligned} \tag{44}$$

where v_x denotes the longitudinal velocity of the vehicle, and the resultant trajectory is a double-lane change maneuver, which is a critical maneuver used for the analysis of vehicle stability, lane-keeping performance, and transient performance.

The path-tracking performance of the autonomous car during cosimulations at a nominal speed of 20 m/s is demonstrated in Figure 3. The evaluation is based on the lateral path deviation as the car follows the desired trajectories corresponding to the DLC maneuver. The lateral displacement with respect to the longitudinal displacement in the global coordinate system obtained by applying the designed controller is depicted in Figure 3. The autonomous vehicle based on the proposed controller demonstrated the capability to swiftly attain the intended trajectories and consistently track the variations of the reference trajectories in terms of lateral displacement compared to the benchmarking BSSTSMC method.

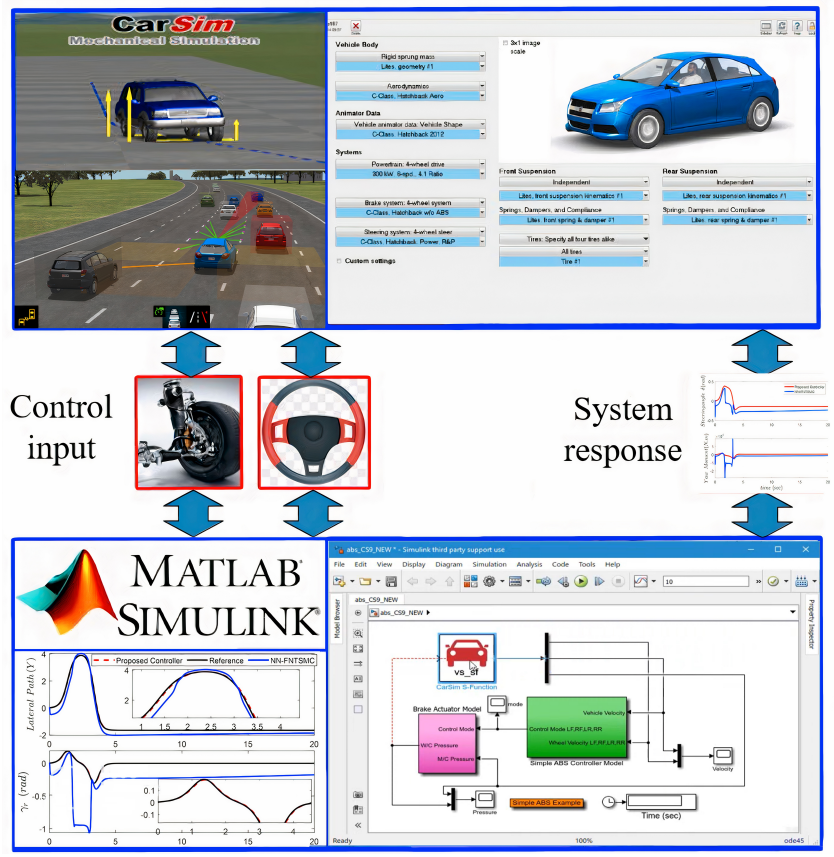

Figure 2. General schematic of the CarSim–Matlab cosimulation framework.

Table 1. Parameters used in the cosimulations [5].

Parameter (unit)	Definition	Value
I_{zz} (kg m^2)	Moment of inertia	2350
m (kg)	Total mass	1485
d_b (m)	Front wheelbase	1.65
$\hat{c}_f$ (N/rad)	Front cornering stiffness	67,500
$\hat{c}_r$ (N/rad)	Rear cornering stiffness	74,500
d_a (m)	Rear wheelbase	1.05

Due to the higher traveling speed, the double-lane change maneuvers are executed in a shorter time, resulting in more critical transient responses. The performance of the proposed controller at different traveling speeds is evaluated using the root mean square error (RMSE) and maximum tracking error, as shown in Table 2. The obtained results indicate that despite the requirement for faster lane-change actions, variations in longitudinal velocity have no impact on the tracking performance indicators.

Table 2. Performance of the proposed controller at various traveling speeds.

	Traveling Speed			
	20 m/s	**30 m/s**	**40 m/s**	**Unit**
y	0.0367	0.0784	0.0985	m
$max(e_y)$	0.0533	0.1125	0.1881	m
ψ	9.3344×10^{-4}	6.7825×10^{-3}	7.2548×10^{-3}	rad
$max(e_\psi)$	0.0025	0.0038	0.0069	rad

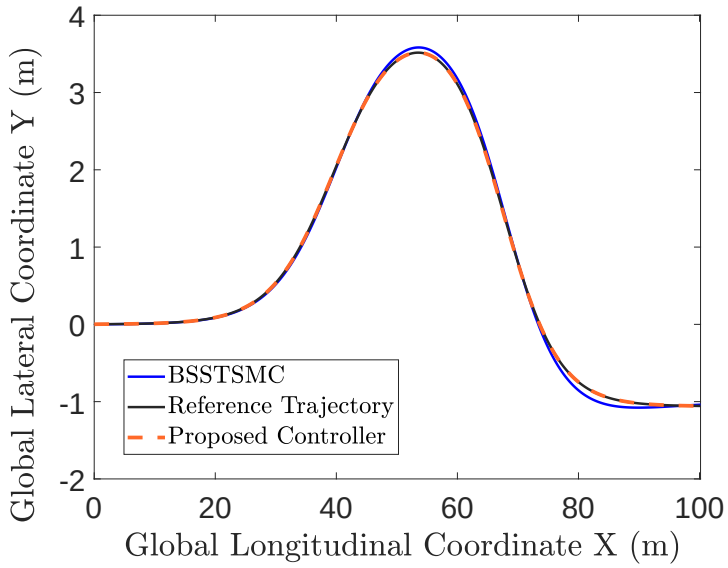

Figure 3. Comparisons of the global lateral position responses of the vehicle with the proposed controller and the benchmarking BSSTSMC approach.

Figure 4 shows the time histories of the yaw-rate tracking performance of the proposed control method compared to the benchmarking BSSTSMC method. It is apparent that, compared to the proposed control scheme, the benchmarking method has difficulty producing the required yaw-rate for the vehicle, and thus the vehicle understeers during the two change of lane actions. Such an understeering performance can pose risk at higher speeds and may cause infringing the lane-keeping task.

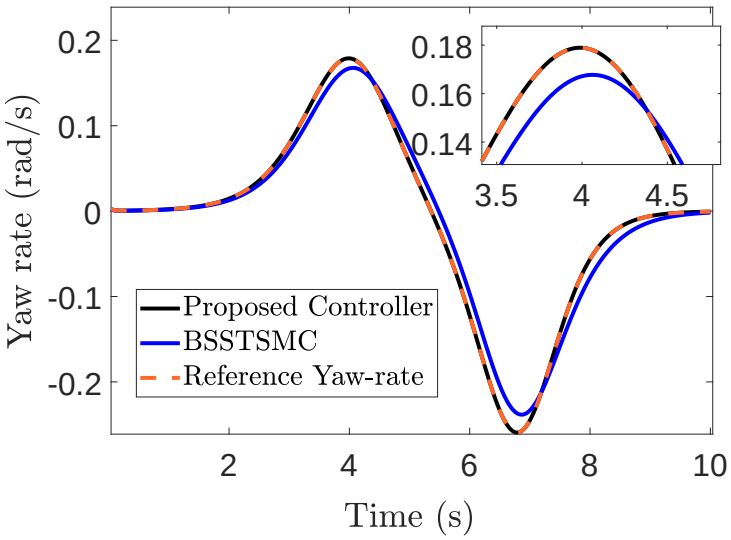

Figure 4. Comparisons of the desired yaw rate tracking performance of the proposed controller and the benchmarking BSSTSMC approach.

Subsequently, apart from the speed variations imposed on the controlled AGV results demonstrated in Table 2, a challenging control situation was created for the road vehicle by lowering friction limit to 0.7 for the tire and road. Additionally, the tire cornering stiffness was modified to $c_f = \hat{c}_f + 4000\sin(6t)$ and $c_r = \hat{c}_r + 4000\sin(6t)$ to add further complexity, together with the force disturbance as a pulsed signal imposed on the vehicle's center of gravity. The performance of the proposed disturbance approximator is evaluated in predicting the disturbances experienced by the vehicle. As such, the total disturbances, together with the approximation performance, is shown in Figure 5, indicating satisfactory

performance. Figure 6 shows the employed control signals, together with the auxiliary compensating signals used to withstand the effect of unknown disturbances. Figure 6 displays bounded and smooth control signals without any chattering for both the steering and yaw moment control.

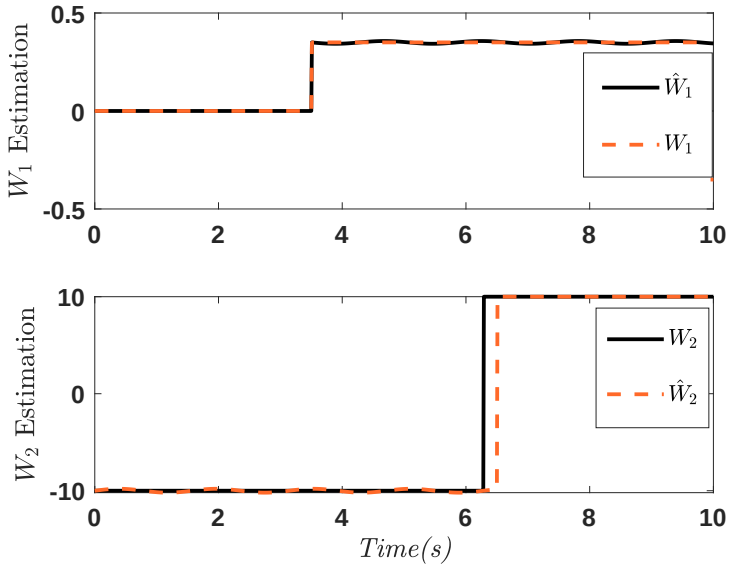

Figure 5. Time histories for the disturbance observer.

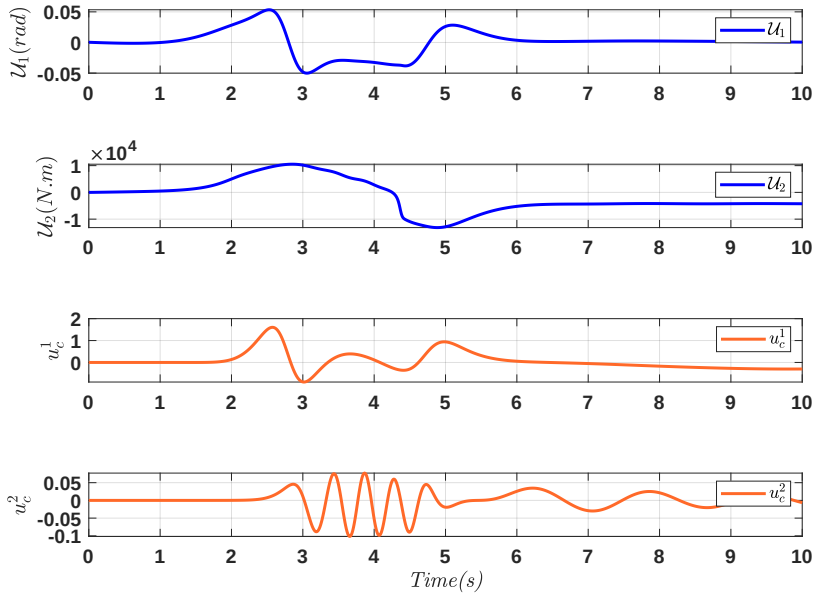

Figure 6. Time histories for control inputs (steering input and DYC) and the compensating control signals.

Finally, to comprehensively assess the efficacy of the proposed control method, a detailed analysis of the AGV's path-tracking performance in the time domain is conducted, and a comparative evaluation is presented against the benchmarking BSSTSMC method. This evaluation, as depicted in Figure 7, provides critical insights into the control strategies' abilities to guide the AGV along the desired trajectory.

In Figure 7, the trajectories generated by both the proposed controller and the BSSTSMC benchmarking method are juxtaposed. This visual representation vividly illustrates the control methods' impact on the AGV's trajectory tracking. Notably, it becomes evident that the AGV under the influence of the proposed controller, as showcased in Figure 6, where the control inputs are depicted, exhibits a significantly enhanced capacity to precisely

adhere to the reference trajectory. The path-tracking trajectory remains remarkably close to the intended path, with minor deviations that are well-contained within acceptable limits.

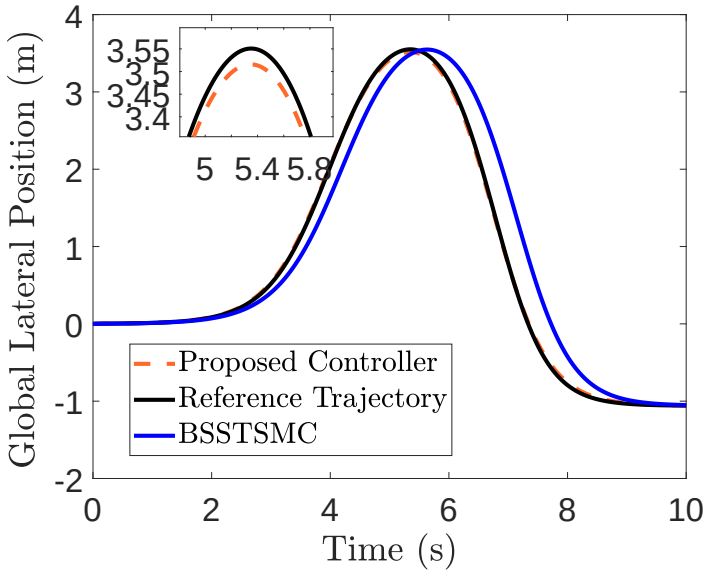

Figure 7. Time histories of the performance of the proposed controller compared to the reference trajectory and the benchmarking BSSTSMC scheme.

In stark contrast, the benchmarking BSSTSMC method exhibits noticeable discrepancies from the reference trajectory. These deviations, as observed in the corresponding trajectory in Figure 7, are more pronounced and extend beyond the desired path. This divergence from the intended trajectory underscores the limitations of the benchmarking method in effectively compensating for the various uncertainties and disturbances inherent in complex AGV scenarios. The larger deviations in the trajectory point to the potential challenges in maintaining accurate path-tracking performance under dynamic and uncertain conditions.

The stark contrast between the proposed controller's trajectory and the benchmarking method's trajectory shown in Figure 7 provides compelling evidence of the superiority of the IBTSMC-based approach. The meticulous integration of integral backstepping and terminal sliding mode control within the proposed framework empowers the AGV with adaptive capabilities, allowing it to effectively mitigate uncertainties and disturbances while adhering closely to the reference trajectory. This adaptive capacity, which is absent in the benchmarking method, emerges as a key differentiator that enables the proposed control strategy to excel in challenging and real-world scenarios.

In summary, the time-domain comparison presented in Figure 7 illuminates the tangible benefits of the proposed IBTSMC controller in ensuring accurate and robust path tracking for AGVs. The designed control inputs shown in Figure 6 play a pivotal role in guiding the AGV along the intended trajectory with minimal deviations. This comparison convincingly demonstrates the effectiveness of the proposed method over the benchmarking BSSTSMC technique, further substantiating the viability of the developed control framework for enhancing the path-tracking performance of autonomous ground vehicles.

5. Conclusions

In this paper, we presented a novel control framework, IBTSMC, for addressing the critical path-tracking task in autonomous ground vehicles (AGVs). The proposed control system, integrating integral backstepping with terminal sliding mode control, effectively handles both structured and unstructured uncertainties.

- **Integral Action for Enhanced Control**: The IBTSMC framework employs continuous adjustments to the control input through integral action, effectively reducing track-

ing errors and elevating the overall tracking performance of autonomous ground vehicles (AGVs).

- **Hybrid Approach for Robustness**: By combining the terminal sliding mode method, the framework ensures finite time convergence; robustness against uncertainties; and a smooth, chatter-free response, which is notably less sensitive to initial conditions.
- **Disturbance Robustness and Validation**: Adaptive control compensators are introduced to counteract external disturbances, guaranteeing the robustness of the system. The proposed control scheme was extensively evaluated via high-fidelity cosimulations utilizing CarSim and MATLAB. Comparative analysis with existing methods confirms the superiority of the proposed controller in path-tracking tasks, showcasing remarkable efficiency across diverse road conditions, uncertainties, and disturbances. The attained global asymptotic stability, supported by the Lyapunov stability theorem, and the finite-time convergence of tracking errors to the origin collectively underscore the dependability and effectiveness of the IBTSMC-based control framework.

Overall, this research contributes to the advancement of autonomous vehicle control by offering a robust and efficient solution for ensuring safety and optimal navigation performance in AGVs. The proposed IBTSMC controller holds potential for real-world applications, providing a foundation for further exploration and implementation in the field of autonomous vehicle technology. However, it is important to note that the presented method may still face challenges in handling extremely complex and unpredictable environments, as well as and faulty sensors and actuators, suggesting potential avenues for future research, particularly merging with fault-tolerant control.

Author Contributions: Conceptualization, H.T. and A.M.; methodology, H.T.; software, H.T. and A.M.; validation, A.M.; investigation, H.T. and A.M.; writing—original draft preparation, H.T. and A.M. All authors have read and agreed to the published version of the manuscript.

Funding: This research received no external funding.

Data Availability Statement: The data presented in this study are available upon request from the corresponding author.

Conflicts of Interest: The authors declare no conflicts of interest.

References

1. Amer, N.H.; Zamzuri, H.; Hudha, K.; Kadir, Z.A. Modelling and control strategies in path tracking control for autonomous ground vehicles: A review of state of the art and challenges. *J. Intell. Robot. Syst.* **2017**, *86*, 225–254. [CrossRef]
2. Hu, C.; Chen, Y.; Wang, J. Fuzzy observer-based transitional path-tracking control for autonomous vehicles. *IEEE Trans. Intell. Transp. Syst.* **2020**, *22*, 3078–3088. [CrossRef]
3. Kim, S.W.; Liu, W.; Ang, M.H.; Frazzoli, E.; Rus, D. The impact of cooperative perception on decision making and planning of autonomous vehicles. *IEEE Intell. Transp. Syst. Mag.* **2015**, *7*, 39–50. [CrossRef]
4. Eskandarian, A.; Wu, C.; Sun, C. Research advances and challenges of autonomous and connected ground vehicles. *IEEE Trans. Intell. Transp. Syst.* **2019**, *22*, 683–711. [CrossRef]
5. Taghavifar, H.; Rakheja, S. Path-tracking of autonomous vehicles using a novel adaptive robust exponential-like-sliding-mode fuzzy type-2 neural network controller. *Mech. Syst. Signal Process.* **2019**, *130*, 41–55. [CrossRef]
6. Dai, Y.; Wang, D. A Tube Model Predictive Control Method for Autonomous Lateral Vehicle Control Based on Sliding Mode Control. *Sensors* **2023**, *23*, 3844. [CrossRef]
7. Kapsalis, D.; Sename, O.; Milanes, V.; Molina, J.J. A reduced LPV polytopic look-ahead steering controller for autonomous vehicles. *Control Eng. Pract.* **2022**, *129*, 105360. [CrossRef]
8. Elbanhawi, M.; Simic, M.; Jazar, R. In the passenger seat: Investigating ride comfort measures in autonomous cars. *IEEE Intell. Transp. Syst. Mag.* **2015**, *7*, 4–17. [CrossRef]
9. Hang, P.; Chen, X.; Luo, F. LPV/H∞ controller design for path tracking of autonomous ground vehicles through four-wheel steering and direct yaw-moment control. *Int. J. Automot. Technol.* **2019**, *20*, 679–691. [CrossRef]
10. Cao, X.; Xu, T.; Tian, Y.; Ji, X. Gain-scheduling LPV synthesis H∞ robust lateral motion control for path following of autonomous vehicle via coordination of steering and braking. *Veh. Syst. Dyn.* **2023**, *61*, 968–991. [CrossRef]
11. Awad, N.; Lasheen, A.; Elnaggar, M.; Kamel, A. Model predictive control with fuzzy logic switching for path tracking of autonomous vehicles. *ISA Trans.* **2022**, *129*, 193–205. [CrossRef]

12. Li, B.; Rakheja, S.; Feng, Y. Enhancement of vehicle stability through integration of direct yaw moment and active rear steering. *Proc. Inst. Mech. Eng. Part D J. Automob. Eng.* **2016**, *230*, 830–840.
13. Mirzaeinejad, H.; Mirzaei, M.; Rafatnia, S. A novel technique for optimal integration of active steering and differential braking with estimation to improve vehicle directional stability. *ISA Trans.* **2018**, *80*, 513–527. [CrossRef]
14. Kang, C.M.; Kim, W.; Chung, C.C. Observer-based backstepping control method using reduced lateral dynamics for autonomous lane-keeping system. *ISA Trans.* **2018** , *27*, 214–226. [CrossRef] [PubMed]
15. Huang, T.; Wang, J.; Pan, H.; Sun, W. Finite-time Fault-tolerant Integrated Motion Control for Autonomous Vehicles with Prescribed Performance. *IEEE Trans. Transp. Electrif.* 2023, *early access*. [CrossRef]
16. Hwang, C.L.; Yang, C.C.; Hung, J.Y. Path tracking of an autonomous ground vehicle with different payloads by hierarchical improved fuzzy dynamic sliding-mode control. *IEEE Trans. Fuzzy Syst.* **2017**, *26*, 899–914. [CrossRef]
17. Swain, S.K.; Rath, J.J.; Veluvolu, K.C. Neural network based robust lateral control for an autonomous vehicle. *Electronics* **2021**, *10*, 510. [CrossRef]
18. Nie, L.; Guan, J.; Lu, C.; Zheng, H.; Yin, Z. Longitudinal speed control of autonomous vehicle based on a self-adaptive PID of radial basis function neural network. *IET Intell. Transp. Syst.* **2018**, *12*, 485–494. [CrossRef]
19. Naranjo, J.E.; Gonzalez, C.; Garcia, R.; De Pedro, T. Lane-change fuzzy control in autonomous vehicles for the overtaking maneuver. *IEEE Trans. Intell. Transp. Syst.* **2008**, *9*, 438–450. [CrossRef]
20. He, S.; Xu, X.; Xie, J.; Wang, F.; Liu, Z. Adaptive control of dual-motor autonomous steering system for intelligent vehicles via Bi-LSTM and fuzzy methods. *Control Eng. Pract.* **2023**, *130*, 105362. [CrossRef]
21. Norouzi, A.; Masoumi, M.; Barari, A.; Farrokhpour Sani, S. Lateral control of an autonomous vehicle using integrated backstepping and sliding mode controller. *Proc. Inst. Mech. Eng. Part K J. Multi-Body Dyn.* **2019**, *233*, 141–151. [CrossRef]
22. Chu, D.; Li, H.; Zhao, C.; Zhou, T. Trajectory tracking of autonomous vehicle based on model predictive control with pid feedback. *IEEE Trans. Intell. Transp. Syst.* **2022**, *24*, 2239–2250. [CrossRef]
23. Chen, G.; Hua, M.; Zong, C.; Zhang, B.; Huang, Y. Comprehensive chassis control strategy of FWIC-EV based on sliding mode control. *IET Intell. Transp. Syst.* **2019**, *13*, 703–713. [CrossRef]
24. Hua, M.; Chen, G.; Zhang, B.; Huang, Y. A hierarchical energy efficiency optimization control strategy for distributed drive electric vehicles. *Proc. Inst. Mech. Eng. Part D J. Automob. Eng.* **2019**, *233*, 605–621. [CrossRef]
25. Wang, P.; Gao, S.; Li, L.; Cheng, S.; Zhao, L. Automatic steering control strategy for unmanned vehicles based on robust backstepping sliding mode control theory. *IEEE Access* **2019**, *7*, 64984–64992. [CrossRef]
26. Taghavifar, H. Robust AISMC-neural network observer-based control of high-speed autonomous vehicles with unknown dynamics. *Proc. Inst. Mech. Eng. Part D J. Automob. Eng.* 2023, *online first*. [CrossRef] .
27. Ao, D.; Huang, W.; Wong, P. K.; Li, J. Robust backstepping super-twisting sliding mode control for autonomous vehicle path following. *IEEE Access* **2021**, *9*, 123165–123177.